Robust Object-based Multi-baseline InSAR

Jian Kang [(1)], Yuanyuan Wang[(1)], Marco Körner[(2)], Xiao Xiang Zhu[(1,3)]

(1) Signal Processing in Earth Observation, Technische Universität München, Arcisstraße 21, 80333 Munich, Germany
(2) Chair of Remote Sensing Technology, Technische Universität München, Arcisstraße 21, 80333 Munich, Germany
(3) Remote Sensing Technology Institute (IMF), German Aerospace Center (DLR), Oberpfaffenhofen, 82234 Weßling, Germany

1. INTRODUCTION

Deformation monitoring by multi-baseline repeat-pass synthetic aperture radar (SAR) interferometry is so far the only imaging-based method to assess millimeter-level deformation over large areas from space. Past research mostly focused on the optimal deformation parameters retrieval on a pixel-basis. Only until recently, the first demonstration of object-based urban infrastructures monitoring by fusing SAR interferometry (InSAR) and the semantic classification labels derived from optical images was presented in [1]–[3]. This paper demonstrates a general framework for object-based InSAR parameters retrieval where the estimation of the parameters is achieved in an object-level instead of pixel-wisely. Furthermore, to handle outliers in real data, a robust phase recovery step in prior to the parameters inversion is also introduced. The proposed method outperforms the current pixel-wised estimators, e.g. periodogram, by a factor of as much as several dozens in the accuracy of the linear deformation estimates.

2. STATE-OF-THE-ART

Multi-baseline SAR interferometry (InSAR) techniques, such as persistent scatterer interferometry (PSI) [4]–[7] and differential SAR tomography (D-TomoSAR) [8]–[10], are the most popular methods for long-term millimeter-level deformation monitoring over large areas. Through modelling the interferometric phase of the scatterers in the SAR image, we are able to reconstruct the 3-D position and the deformation history of individual scatterers.

The research on multi-baseline InSAR has been mainly based on two fundamental cases of scattering model: persistent scatterer (PS), and distributed scatterer (DS). The main focus was put on the optimum retrieval of the phase history parameters of the individual scatterers. On one hand, persistent scatterer interferometry (PSI) has been demonstrated to efficiently identify individual coherent targets, as well as retrieving their phase history parameters [4]–[6]. Methods have also been proposed to use closely spaced PS pairs [11], [12] to increase the density of the PSs. On the other hand, DS-based methods were also proposed to use interferograms of only short temporal and spatial baselines [13], as well as to apply adaptive multi-looking on the DSs such as SqueeSAR

[14], [15] and nonlocal-InSAR (NL-InSAR) [16], [17].

The abovementioned techniques are either only inversion on individual single pixel, or based on a weighted average of pixels where the natural geometric and semantic information in the SAR image has not been explicitly exploited. In another word, none of the abovementioned algorithms has addressed the joint retrieval of geophysical parameters given certain geometric information, such as an object mask within which the height and the deformation parameters may share certain prior knowledge, e.g. smoothness, sparsity. In this paper, we demonstrate an mathematical model that coherently integrates the a priori geometric information into the parameters inversion.

3. OBJECT-BASED MULTI-BASELINE INSAR

3.1 Single-pixel multi-baseline InSAR model

The time series of the interferometric phase in a SAR image stack is determined by the elevation of the pixel, as well as its deformation over the observed period. For example, a PS time series $\mathbf{g}(s,d)$ can be modeled as:

$$\bar{\mathbf{g}}(s,d) = A\exp\left\{-j\frac{4\pi}{\lambda}\left(\frac{s}{r}\times\mathbf{b}+d\times\mathbf{p}\right)\right\} \tag{1}$$

where A is the modeled amplitude of the PS, $\mathbf{b}$ is the vector of the spatial baseline, $\mathbf{p}$ is the vector of the deformation model, e.g. $\mathbf{p}=\mathbf{t}$ for linear motion, and $\mathbf{p}=\sin\left(2\pi(\mathbf{t}-t_0)\right)$ for the seasonal motion model with the temporal baseline $\mathbf{t}$, s and d are the unknown elevation and the deformation parameters to be estimated, respectively, λ is the wavelength of the radar transmitted signals, and r denotes the range between the radar and the observed object. Since we mainly focus on the complex phase of strong PSs, the amplitude has been removed in the following study.

The parameters s and d can be solved by the maximum likelihood estimator (MLE)

$$\left\{\hat{s},\hat{d}\right\} = \arg\min_{s,d}\left\|\mathbf{g}-\bar{\mathbf{g}}(s,d)\right\|_2^2 \tag{2}$$

where $\mathbf{g}$ is the observed PS phase time series, and $\hat{s},\hat{d}$ represents the estimated elevation and deformation, respectively. This is equivalent to the periodogram [18], [19]

$$\left\{\hat{s},\hat{d}\right\} = \arg\max_{s,d}\left|\bar{\mathbf{g}}(s,d)^H\,\mathbf{g}\right| \tag{3}$$

3.2 Object-level multi-baseline InSAR model

Given a spatial neighborhood of pixels of the same object, e.g. the flat roof of a building, its interferometric phase stack can be represented by a 3-mode tensor $\mathcal{G}\in\mathbb{C}$, where I_1, I_2 represent the spatial dimension in

range and azimuth, and I_3 denotes the number of SAR images. Similar to equation (1), its tensor extension can be expressed as follows:

$$\bar{\mathcal{G}}(\mathbf{S},\mathbf{D}) = \exp\left\{-j\frac{4\pi}{\lambda}\left(\frac{1}{r}\mathbf{S}\otimes\mathbf{b}+\mathbf{D}\otimes\mathbf{p}\right)\right\} \tag{4}$$

Here, $\bar{\mathcal{G}}$ is the modeled complex phase tensor of the object, $\mathbf{S}$ and $\mathbf{D}$ represent the matrices of elevation and deformation to be estimated, respectively. The symbol $\otimes$ denotes the outer product, which plays a role for the dimension extension [20]. The interpretation is illustrated in Figure 1.

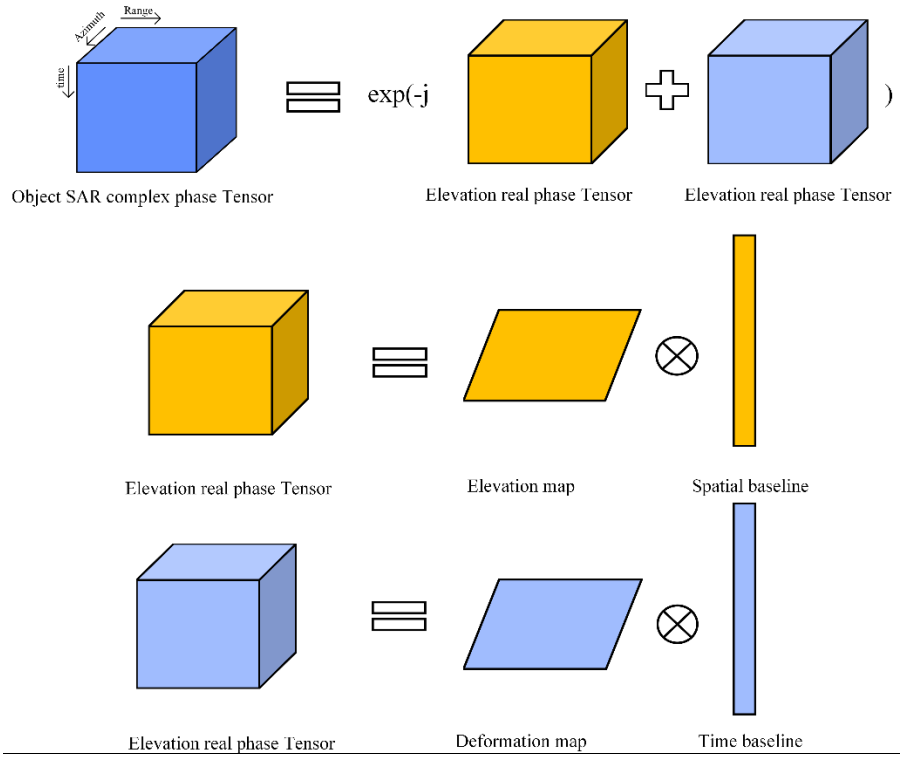

Figure 1 InSAR complex phase stack with the tensor model

Given the observed complex phase tensor $\mathcal{G}$ of a certain object, the goal is to jointly reconstruct the parameters of all the pixels. In the proposed method, we exploit the prior knowledge of their spatial deformation pattern, e.g. smoothness, sparsity. To this end, the optimization problem of equation (2) is extended to the following expression:

$$\left\{\hat{\mathbf{S}},\hat{\mathbf{D}}\right\} = \arg\min_{\mathbf{S},\mathbf{D}} \frac{1}{2}\left\|\mathcal{W}\circ\ \mathcal{G}\quad \mathcal{G}\ \ \tilde{\mathbf{S}},\mathbf{D})\right\|_F^2 + \alpha f(\mathbf{S},\mathbf{D}) \tag{5}$$

where $\mathcal{W}$ denotes a weighting tensor, $\circ$ denotes the element-wise product between two tensors, and α is a regularization parameter of the prior $f(\mathbf{S},\mathbf{D})$. The first term is the weighted data fidelity term which calculates the weighted Frobenius norm of the log likelihood between observed tensor $\mathcal{G}$. The weighting tensor captures

different phase variance of the pixels in the object. $f(\mathbf{S},\mathbf{D})$ denotes the penalty term which represents the spatial prior of **S** and **D**. Therefore, equation (5) is also the *maximum a posterior* (MAP) estimator of **S** and **D** for complex Gaussian distributed observations.

One popular smoothness prior is total variation (TV) norm which is utilized in multiple image processing problems, e.g. image deblurring, denoising and inpainting [21]–[23]. Therefore, we exploit TV norm as the penalty term in our work and the optimization in equation (5) can be written as:

$$\left\{\hat{\mathbf{S}},\hat{\mathbf{D}}\right\}=\arg\min_{\mathbf{S},\mathbf{D}}\frac{1}{2}\left\|\mathcal{W}\circ\mathcal{G}-\mathcal{G}(\mathbf{S},\mathbf{D})\right\|_F^2+\alpha\sum_{i,j}\left|\mathbf{D}(i+1,j)-\mathbf{D}(i,j)\right|+\left|\mathbf{D}(i,j+1)-\mathbf{D}(i,j)\right| \tag{6}$$

where i,j are the pixel row and column coordinates of the matrix.

Equation (6) requires the minimization of a nonlinear and nonconvex function. It can be solved by the limited memory quasi Newton method – Broyden–Fletcher–Goldfarb–Shanno (LBFGSB) [24]–[26] which is developed for unconstrained nonlinear optimization. It has recently been applied as a comparison solver for nonconvex optimization in [27] and utilized as an efficient solver for patch-ordering regularization inverse problem [28].

3.3 Robust object-based InSAR deformation reconstruction

In real data, the observed data stack $\mathcal{G}$ may contain outliers against which the abovementioned MAP is not robust. Therefore, inspired by [29] which gives a thorough analysis of exploiting low rank information for multi-temporal SAR datasets, the abovementioned approach is extended to a robust version in case outliers exist. In the robust approach, a preliminary object-based phase recovery step is applied to the observed phase stack $\mathcal{G}$, before the joint parameter reconstruction. Afterwards, the abovementioned reconstruction approach is applied.

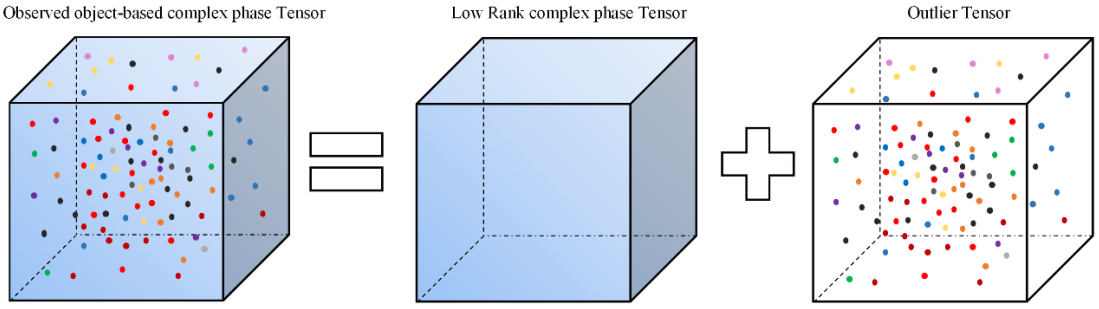

Figure 2 Robust Low Rank Tensor Decomposition for the observed object-based complex phase tensor

In the object-based phase recovery step, as shown in Figure 2, we first decompose the observed phase tensor $\mathcal{G}$ into two parts: one is the low-rank tensor part $\mathcal{A}$ and the other is the sparse outlier tensor part $\mathcal{E}$, because the outlier-free complex phase stack $\mathcal{A}$ can be considered as a low rank tensor compared to the observed phase tensor $\mathcal{G}$. Estimating $\mathcal{A}$ leads to the following optimization problem:

$$\left\{\hat{\mathcal{A}},\hat{\mathcal{E}}\right\}=\arg\min_{\hat{\mathcal{A}},\hat{\mathcal{E}}} Trank\left(\mathcal{A}\right)+\beta\left\|\mathcal{E}\right\|_0,\quad s.t.\ \mathcal{A}+\mathcal{E}=\mathcal{G} \tag{7}$$

where $Trank\left(\mathcal{A}\right)$ describes the Tucker Rank [20], [30] of $\mathcal{A}$, the outliers are modeled by the tensor L_0 norm, and β is the regularization parameter. Since it is a NP-hard problem which could not be solved efficiently, it is relaxed by the convex optimization model [31]:

$$\left\{\hat{\mathcal{A}},\hat{\mathcal{E}}\right\}=\arg\min_{\hat{\mathcal{A}},\hat{\mathcal{E}}} \sum_{n=1}^{N}\left\|\mathbf{A}_{(n)}\right\|_*+\gamma\left\|\mathcal{E}\right\|_1,\ s.t.\ \mathcal{A}+\mathcal{E}=\mathcal{G} \tag{8}$$

where $Trank\left(\mathcal{A}\right)$ is replaced by the convex relaxation, i.e. nuclear norm of tensor $\mathcal{A}=\sum_{n=1}^{N}\left\|\mathbf{A}_{(n)}\right\|_*$, which is the sum of the N nuclear norms $\left\|\mathbf{A}_{(n)}\right\|_*$ of the mode-n unfoldings, $n=1,\cdots N$ of $\mathcal{A}$; and $\left\|\mathcal{E}\right\|_0$ is replaced by $\left\|\mathcal{E}\right\|_1$. The regularization parameter γ controls the balance between the decomposed low rank part and outlier part.

The solution of the equation (8) can be efficiently solved by an alternating direction augmented Lagrangian (ADAL) method proposed in [31]. After the outliers have been discarded in the retrieved tensor $\mathcal{A}$, we can regard it as the input for (5) and obtain the deformation matrix in an object-level.

4. EXPERIMENTS

A multi-baseline SAR image stack with the spatial deformation pattern shown in Figure 3 was simulated as the ground truth. The linear deformation rate ranges from 1 mm/year to 2.5 mm/year. We choose a spatial baseline comparable to that of TerraSAR-X and a temporal baseline with regular spacing from 0 to 5 (years). The number of images is 20. Uncorrelated complex circular Gaussian noise is added to the simulated SAR image stacks with the signal-to-noise ratio (SNR) of 0dB and 5dB, respectively. Since we do not simulate the outliers in this simulation, we directly exploit the proposed approach without robust low rank phase preprocessing, and compare the performance with the pixel-wise periodogram and pixel-wise periodogram + direct TV filtering on the real-valued estimates, which is illustrated in Figure 3.

As shown from the results, the pixel-wise periodogram result (the second column in Figure 3) is much noisier comparing to the other two methods. Especially, in case of the lower SNR (0dB), the result got by pixel-wise periodogram cannot even be easily interpreted. What is more interesting is the comparison between the proposed method and pixel-wise periodogram + TV. Here, the pixel-wise periodogram + TV refers to a direct TV filtering [32] on the pixel-wise periodogram estimates instead of optimizing the periodogram and the TV term jointly as done in the proposed algorithm. The results show that applying TV filtering afterwards can also achieve certain level of denoising, especially for high SNR observations. However, when the SNR is low, more errors and biases existed in the result obtained by pixel-wise periodogram will severely influence the performance of TV filtering. A quantitative comparison of the performance of the abovementioned three algorithms is listed in Table 1. The proposed approach outperforms the single-pixel one by a factor of over 40.

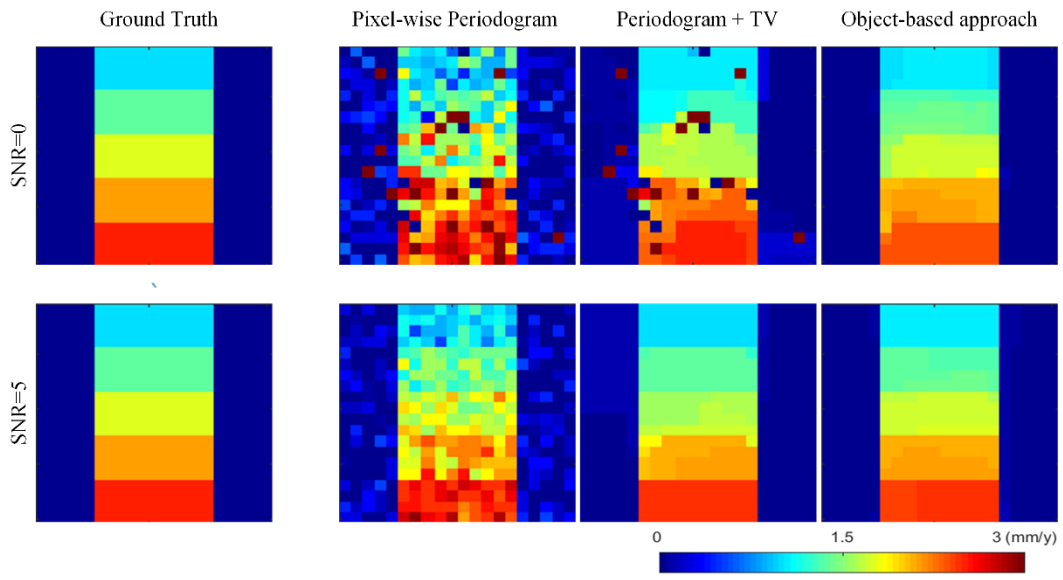

Figure 3. Left: simulated ground truth of deformation map, and right: the results estimated by pixel-wise periodogram, periodogram + TV on the real-valued estimates, and the proposed object-based approach. The color represents the yearly linear deformation rate. We can see that introducing a TV term, no matter directly applied on the real-valued single-pixel estimates or coherently employed within the joint inversion, improved the estimates greatly. The advantage of employing TV in the joint inversion is more prominent for low SNR, as the proposed approach almost perfectly reconstructed the deformation signal at 0dB.

Table 1 numerical performance for the results shown in Figure 3

		pixel-wise periodogram	pixel-wise periodogram + TV	proposed approach
Standard Deviation [mm/year]	SNR = 0dB	2.64	2.39	**6.32e-2**
	SNR = 5dB	2.31e-1	6.72e-2	**3.94e-2**

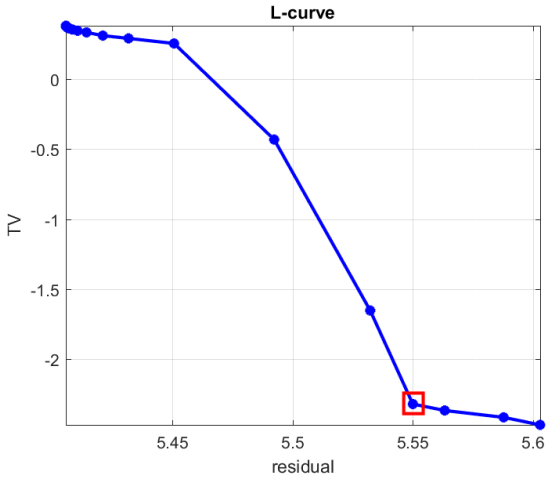

Figure 4 Optimal regularization parameter chosen by L-curve plot (Simulated case: SNR=0dB)

The parameter α can be determined by L-curve method, which is a plot of the size of the regularized term versus the size of the corresponding data fidelity residual for all valid regularization parameters [33]. Generally, the L-curve is made up of a

"flat" part and a "vertical" part. The optimal parameter is decided by the corner point of the L-curve which produces maximum curvature of the curve. Concretely, we plot an L-curve example which is illustrated in Figure 4 and the corresponding α is chosen as 350 and the noise level is set with SNR=0dB.

Moreover, to investigate the robust object-based deformation reconstruction approach, we simulate uniformly distributed random phase noise to 20% of the pixels. The estimation results is shown in Figure 5. The SNR of the outlier-free observation is set to 5dB. The regularization parameter α is set to 300 in the robust object-based deformation reconstruction. And the value γ is set to 0.7 which is tuned to maintain the good balance of outlier removal and detail retention. The detailed parameter selection for γ can be found in [31]. The result of the pixel-wise approach contains both the noise and outliers. Although the afterwards TV filtering can mitigate most of the noise, the outliers remains. However, the proposed robust algorithm achieves much more reliable result than the previous two methods.

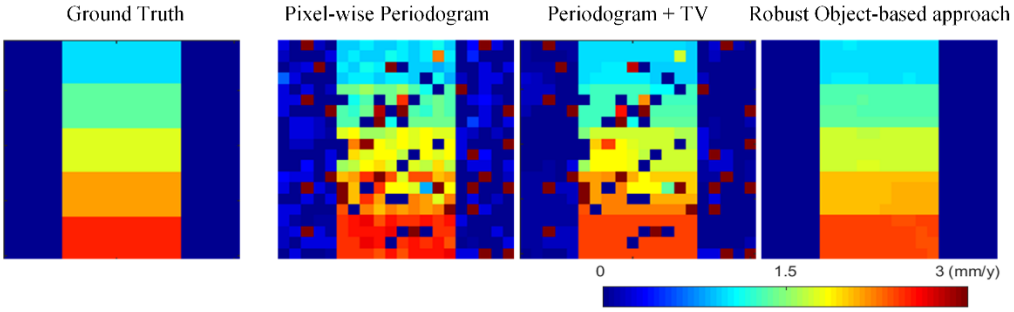

Figure 5 The results obtained by the pixel-wise periodogram, periodogram + TV, and robust object-based approach in case of the whole data added by complex Guassian noise (SNR=5dB) and 20% percentage of data corrupted by uniformly distributed random phase outliers.

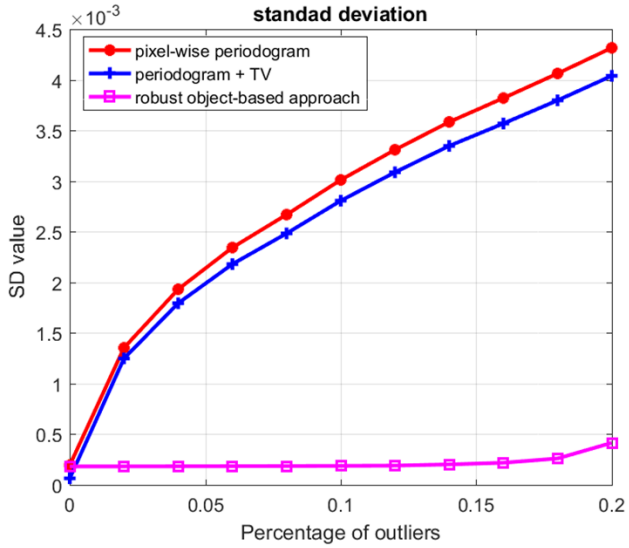

Figure 6. Standard deviation of the estimate from pixel-wise periodogram, periodogram+TV and the robust object-based algorithm at different outlier percentages in the observations.

We also make the numerical analysis to compare pixel-wise peridodogram, peridodogram+TV and the robust object-based

approach under different percentages of outliers. Figure 6 presents the numerical study of the three different algorithms. It is shown that the pixel-wise periodogram and peridodogram+TV are very sensitive to outliers, however, the proposed algorithm can robustly reconstruct the deformation map with small error.

5. SUMMARY

We demonstrated a new mathematical framework of robust object-based parameters retrieval in multi-baseline InSAR. We demonstrated that by introducing an prior term in the inversion, the accuracy of the estimates can be improved by a factor of over 40 for outlier-free observations at 0dB. This improvement factor is even higher if outlier exists in the observation. This framework is one promising development of multibaseline InSAR, as it moves parameters retrieval on single-pixel to an object-level which explores the geometric information as a nature in any kind of image besides the interferometric phase measurement observed at each pixel. This framework can greatly help the application of deformation monitoring, 3-D city model reconstruction from InSAR point cloud, and so on.

REFERENCE

[1] Y. Wang and X. X. Zhu, "Fusing Meter-Resolution 4-D InSAR Point Clouds and Optical Images for Semantic Urban Infrastructure Monitoring," *IEEE Trans. Geosci. Remote Sens.*, 2016.

[2] Y. Wang and X. X. Zhu, "InSAR Forensics: Tracing InSAR Scatterers in High Resolution Optical Image," presented at the Fringe 2015, 2015.

[3] Y. Wang and X. X. Zhu, "Semantic Fusion of SAR Interferometry and Optical Image with Application to Urban Infrastructure Monitoring," presented at the La Grande Motte, France, La Grande Motte, France, 2015.

[4] A. Ferretti, C. Prati, and F. Rocca, "Permanent scatterers in SAR interferometry," *IEEE Trans. Geosci. Remote Sens.*, vol. 39, no. 1, pp. 8–20, Jan. 2001.

[5] N. Adam, B. Kampes, M. Eineder, J. Worawattanamateekul, and M. Kircher, "The development of a scientific permanent scatterer system," in *ISPRS Workshop High Resolution Mapping from Space, Hannover, Germany*, 2003, vol. 2003, p. 6.

[6] S. Gernhardt and R. Bamler, "Deformation monitoring of single buildings using meter-resolution SAR data in PSI," *ISPRS J. Photogramm. Remote Sens.*, vol. 73, pp. 68–79, Sep. 2012.

[7] M. K. Bert, "Radar Interferometry: Persistent Scatterers Technique," *Neth. Springer*, 2006.

[8] X. X. Zhu and R. Bamler, "Very High Resolution Spaceborne SAR Tomography in Urban Environment," *IEEE Trans. Geosci. Remote Sens.*, vol. 48, no. 12, pp. 4296–4308, Dec. 2010.

[9] X. X. Zhu and R. Bamler, "Tomographic SAR Inversion by L_{1} -Norm Regularization—The Compressive Sensing Approach," *IEEE Trans. Geosci. Remote Sens.*, vol. 48, no. 10, pp. 3839–3846, Oct. 2010.

[10] G. Fornaro, S. Verde, D. Reale, and A. Pauciullo, "CAESAR: An approach based on covariance matrix decomposition to improve multibaseline–multitemporal interferometric SAR processing," *Geosci. Remote Sens. IEEE Trans. On*, vol. 53, no. 4, pp. 2050–2065, 2015.

[11] Y. Wang, X. Zhu, and R. Bamler, "An Efficient Tomographic Inversion Approach for Urban Mapping Using Meter Resolution SAR Image Stacks," *IEEE Geosci. Remote Sens. Lett.*, vol. 11, no. 7, pp. 1250–1254, 2014.

[12] M. Costantini, S. Falco, F. Malvarosa, F. Minati, F. Trillo, and F. Vecchioli, "Persistent scatterer pair interferometry: approach and application to COSMO-SkyMed SAR data," *IEEE J. Sel. Top. Appl. Earth Obs. Remote Sens.*, vol. 7, no. 7, pp. 2869–2879, 2014.

[13] P. Berardino, G. Fornaro, R. Lanari, and E. Sansosti, "A new algorithm for surface deformation monitoring based on small baseline differential SAR interferograms," *IEEE Trans. Geosci. Remote Sens.*, vol. 40, no. 11, pp. 2375–2383, 2002.

[14] A. Ferretti, A. Fumagalli, F. Novali, C. Prati, F. Rocca, and A. Rucci, "A New Algorithm for Processing Interferometric Data-Stacks: SqueeSAR," *IEEE Trans. Geosci. Remote Sens.*, vol. 49, no. 9, pp. 3460–3470, Sep. 2011.

[15] Y. Wang, X. Zhu, and R. Bamler, "Retrieval of Phase History Parameters from Distributed Scatterers in Urban Areas Using Very High Resolution SAR Data," *ISPRS J. Photogramm. Remote Sens.*, vol. 73, pp. 89–99, Sep. 2012.
[16] C.-A. Deledalle, L. Denis, and F. Tupin, "NL-InSAR: Nonlocal interferogram estimation," *Geosci. Remote Sens. IEEE Trans. On*, vol. 49, no. 4, pp. 1441–1452, 2011.
[17] X. X. Zhu, R. Bamler, M. Lachaise, F. Adam, Y. Shi, and M. Eineder, "Improving TanDEM-X DEMs by Non-local InSAR Filtering," in *EUSAR 2014; 10th European Conference on Synthetic Aperture Radar; Proceedings of*, 2014, pp. 1–4.
[18] D. Rife and R. R. Boorstyn, "Single tone parameter estimation from discrete-time observations," *Inf. Theory IEEE Trans. On*, vol. 20, no. 5, pp. 591–598, 1974.
[19] Y. Wang and X. X. Zhu, "Robust Estimators for Multipass SAR Interferometry," *IEEE Trans. Geosci. Remote Sens.*, vol. 54, no. 2, pp. 968–980, Feb. 2016.
[20] A. Cichocki *et al.*, "Tensor decompositions for signal processing applications: From two-way to multiway component analysis," *Signal Process. Mag. IEEE*, vol. 32, no. 2, pp. 145–163, 2015.
[21] M. Zhu and T. Chan, "An efficient primal-dual hybrid gradient algorithm for total variation image restoration," *UCLA CAM Rep.*, pp. 8–34, 2008.
[22] M. Tao, J. Yang, and B. He, "Alternating direction algorithms for total variation deconvolution in image reconstruction," *TR0918 Dep. Math. Nanjing Univ.*, 2009.
[23] A. Chambolle and T. Pock, "A first-order primal-dual algorithm for convex problems with applications to imaging," *J. Math. Imaging Vis.*, vol. 40, no. 1, pp. 120–145, 2011.
[24] C. Zhu, R. H. Byrd, P. Lu, and J. Nocedal, "L-BFGS-B: FORTRAN subroutines for large scale bound constrained optimization," *Rep. NAM-11 EECS Dep. Northwest. Univ.*, 1994.
[25] R. H. Byrd, P. Lu, J. Nocedal, and C. Zhu, "A limited memory algorithm for bound constrained optimization," *SIAM J. Sci. Comput.*, vol. 16, no. 5, pp. 1190–1208, 1995.
[26] C. Zhu, R. H. Byrd, P. Lu, and J. Nocedal, "Algorithm 778: L-BFGS-B: Fortran Subroutines for Large-scale Bound-constrained Optimization," *ACM Trans Math Softw*, vol. 23, no. 4, pp. 550–560, Dec. 1997.
[27] P. Ochs, Y. Chen, T. Brox, and T. Pock, "iPiano: Inertial proximal algorithm for nonconvex optimization," *SIAM J. Imaging Sci.*, vol. 7, no. 2, pp. 1388–1419, 2014.
[28] G. Vaksman, M. Zibulevsky, and M. Elad, "Patch Ordering as a Regularization for Inverse Problems in Image Processing," *SIAM J. Imaging Sci.*, vol. 9, no. 1, pp. 287–319, 2016.
[29] W. Lingyun, "Quantification of Low-rank Information in Multi-temporal SAR Datasets," Technical University of Munich, 2015.
[30] T. G. Kolda and B. W. Bader, "Tensor decompositions and applications," *SIAM Rev.*, vol. 51, no. 3, pp. 455–500, 2009.
[31] D. Goldfarb and Z. Qin, "Robust low-rank tensor recovery: Models and algorithms," *SIAM J. Matrix Anal. Appl.*, vol. 35, no. 1, pp. 225–253, 2014.
[32] T. Goldstein and S. Osher, "The split Bregman method for L1-regularized problems," *SIAM J. Imaging Sci.*, vol. 2, no. 2, pp. 323–343, 2009.
[33] P. C. Hansen and D. P. O'Leary, "The use of the L-curve in the regularization of discrete ill-posed problems," *SIAM J. Sci. Comput.*, vol. 14, no. 6, pp. 1487–1503, 1993.